Pure Appl. Chem., Vol. 72, Nos. 1–2, pp. 91–99, 2000.

Phototransformation of alkanethiol-derivatized noble metal nanoparticles*

Chil Seong Ah, Hyouk Soo Han, Kwan Kim, and Du-Jeon Jang†

School of Chemistry and Center for Molecular Catalysis, Seoul National University, Seoul 151-742, Korea

Abstract: Photon-initiated shape transformation of *n*-alkanethiol-derivatized noble metal nanoparticles has been studied with variations of metal, alkanethiol, and solvent. Silver nanoparticles undergo fragmentation upon irradiation while gold ones barely do. Silver/gold composite particles follow the case of silver with a reduced efficiency. The efficiency decreases as alkanethiol length or solvent dipole moment increases. Following the conduction of thermalized photon energy, alkanethiol can dissociate in a period of heat dissipation, and some of dethiolated particles fragment within the recombination time. Prior to the thermal conduction, shape transformation via melt and vaporization also occurs for both metals but this effect is less apparent for silver because of more notable fragmentation followed. The difference in the transformation of two metals is ascribed to the differences in work function, oxidation potential, atomization enthalpy, and particle size. Smaller fragmentation efficiency with more polar solvent or longer alkanethiol is attributed mainly to relatively smaller dissociation rate compared with heat dissipation rate.

INTRODUCTION

Nanoparticles have a variety of unique spectroscopic, electronic, and chemical properties that geminate from their small sizes and high surface/volume ratios [1–4]. Particularly, excellent catalytic activity is known to exist in nanoparticles, correlating with their sizes and shapes [5,6]. Many studies on colloidal nanoparticles have thus been focused on the control of their sizes, shapes, and growth kinetics [7–19] as well as on the characterization of their chemical and physical properties [3,20–22].

Noble metal nanoparticles attract great interest because of their current and future applications not only in the field of catalysts but also in the development of efficient sensors, drug deliverers, opto-electronics, and magnetic devices [5,23–26]. They exhibit new optical properties [1,2,27–29] which are observed neither in molecules nor in bulk metals. One particular example is the presence of a strong absorption band in the visible region, caused by the surface plasmon oscillation modes of conduction electrons that are coupled through the surface to external electromagnetic field. The optical properties of platinum, palladium, silver, and gold colloidal nanoparticles thus have received considerable attention [4,20–22,30–41]. In fact, the color of the noble metal nanoparticles is known to depend on both the sizes and shapes of the particles as well as on the refractive index of the surrounding medium [27]. For instance, in the region of intrinsic size, in contrast to extrinsic size, the plasmon absorption spectrum becomes broader, with a smaller absorbance, as the average particle size decreases [1,42]. The wavelength and absorbance of the spectrum are also reported to depend on the nature and the concentration of adsorbed species [40,41,43].

Pure Appl. Chem.* **72, 1–331 (2000). An issue of reviews and research papers based on lectures presented at the 1st IUPAC Workshop on Advanced Materials (WAM1), Hong Kong, July 1999, on the theme of nanostructured systems.
†Corresponding author (djjang@plaza.snu.ac.kr).

Upon derivatization with organic molecules, nanoparticles can be dissolved in various solvents, extending their application capabilities [4,44]. Alkanethiolization of metal nanoparticles occurs with forming a covalent bond between the sulfur atom of alkanethiol and the surface of particles or with chemisorbing to the metal particle by donating electron cloud to the thiolate functional group.

Some types of noble metal nanoparticles are reported to undergo optical or thermal shape transformation. While photoexcited silver nanoparticles suspended in water are reported to experience electron ejection and subsequent disintegration [3], laser-induced size reduction of gold nanoparticles in water has been explained to occur via melting and vaporization [20,21]. Energetically unstable gold nanorods are reported to undergo thermal decomposition as well as photothermal melting and fragmentation [10,46].

In this report, we present the experimental observations made on the photophysical and photochemical shape transformation of *n*-alkanethiol-derivatized noble metal nanoparticles in organic solvent. The results clearly show that the shape of nanoparticles changes upon irradiation, but the transformation depends on metal and solvent as well as on alkanethiol.

EXPERIMENTAL

Samples of *n*-alkanethiol-derivatized noble nanoparticles were prepared via a two-phase synthetic route, and the detailed procedures have been described previously [44]. The typical diameters of silver, silver/gold, and gold nanoparticles were measured to be 6.2 nm, 2.5 nm, and 2.2 nm, respectively. Their shapes were all to be faceted polyhedral rather than spherical [44]. For the bimetallic silver/gold nanoparticles, the average atomic molar ratio of Ag to Au was 1; however, silver atoms were found to be enriched in the outer part [28,34].

A drop of colloid sample was spread on a carbon coated-copper grid to take the transmission electron microscopic (TEM) images of colloids. The TEM images obtained using a microscope (JEOL, JEM2000) were used to determine the particle sizes of nanoparticles. Absorption spectral change with irradiation was monitored by measuring the absorption spectra of a 3-mL sample in a quartz cell of 1.0-cm path length at scheduled intervals quickly with a UV/vis spectrophotometer (Sinco, UVS2040). The sample was irradiated with 355-nm, 30-ps pulses of a mode-locked Nd:YAG laser (Quantel, YG501) run at 10 Hz with a spot diameter of 8 mm.

Picosecond transient absorption kinetic profiles were measured by using the same laser and a CCD (Princeton Instruments, RTE128H)-attached 10 ps streak camera (Hamamatsu, C2830). Laser pulses of 355 nm with a typical energy of 0.8 mJ were directed, with a spot diameter of 2 mm, to a sample contained in a quartz cell of 2-mm path length. Fluorescence from an organic dye, excited with pulses split from the sample excitation laser beam, was detected using the streak camera. The comparison of the dye emission kinetic profiles obtained with and without sample excitation yields a transient absorption kinetic profile [45]. Kinetic profiles in long time windows, i.e., beyond the largest window of the streak camera (10 ns), were obtained by connecting the kinetic profiles measured at different optical delays. Kinetic constants were extracted by fitting observed kinetics profiles to computer-simulated profiles convoluted with the appropriate instrument response functions.

RESULTS AND DISSCUSION

As can be seen in Fig. 1, the absorption spectra of *n*-dodecanethiol-derivatized noble metal nanoparticles are all to change continuously with irradiation. The spectral changes are, however, quite dependent on the metal composition. The plasmon absorption band of AgC_{12} becomes broader upon irradiation; it decreases in the blue wavelength region while it increases in the red. In contrast, the absorption band of AuC_{12} becomes narrower, resulting in increased absorption at the peak maximum wavelength as well as

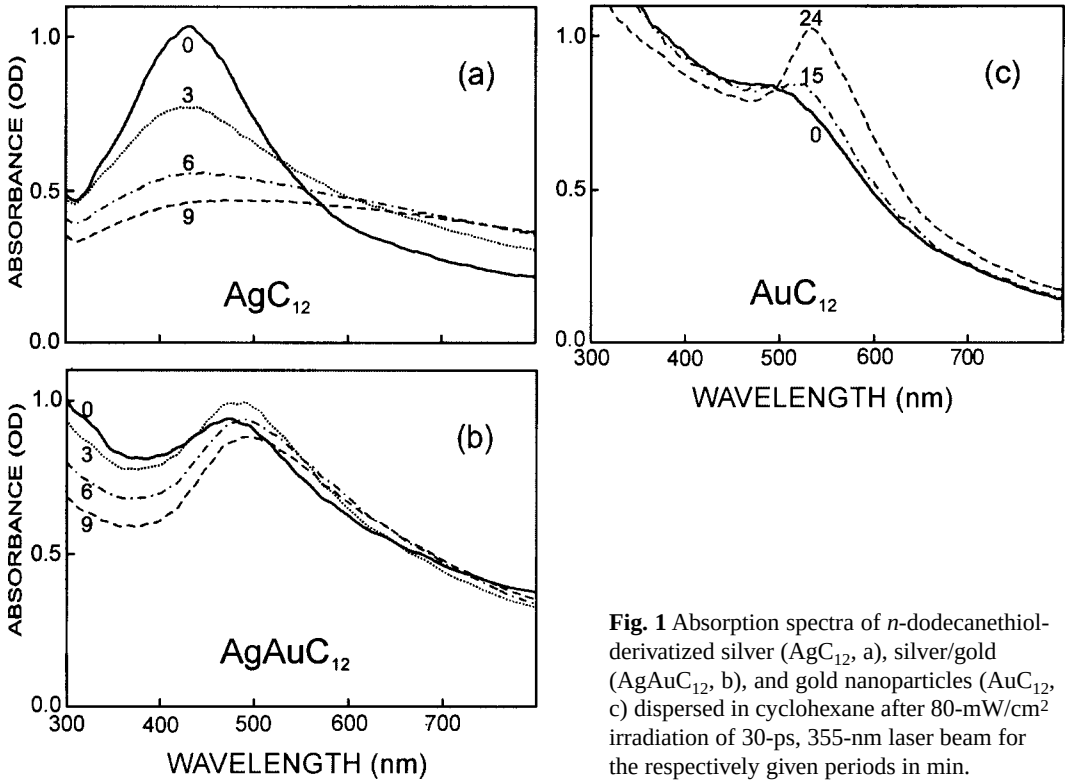

Fig. 1 Absorption spectra of *n*-dodecanethiol-derivatized silver (AgC_{12}, a), silver/gold ($AgAuC_{12}$, b), and gold nanoparticles (AuC_{12}, c) dispersed in cyclohexane after 80-mW/cm^2 irradiation of 30-ps, 355-nm laser beam for the respectively given periods in min.

at the red. For the bimetallic $AgAuC_{12}$, the absorption change is partly similar to those of AgC_{12} and AuC_{12}. At the beginning, the plasmon absorption is to increase at the peak maximum as in AuC_{12}, but it becomes smaller along with the irradiation as in AgC_{12}. As can be seen in Fig. 2, the absorption spectrum of AgC_{18} is also to change with irradiation as in AgC_{12}, albeit the extent of change is far smaller than in AgC_{12}.

As one may expect from the spectral changes in Figs. 1 and 2, the TEM images shown in Fig. 3 illustrate that a shape transformation takes place upon irradiation for all kinds of *n*-alkanethiol-derivatized noble metal nanopaticles. The TEM images also indicate that the pattern as well as the efficiency of the

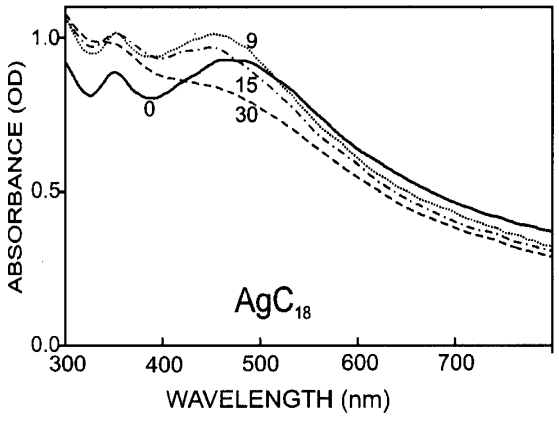

Fig. 2 Absorption spectra of *n*-octadecanethiol-derivatized silver nanoparticles (AgC_{18}) in cyclohexane after 80 mW/cm^2 irradiation of 30 ps, 355 nm laser beam for the respectively shown periods in min.

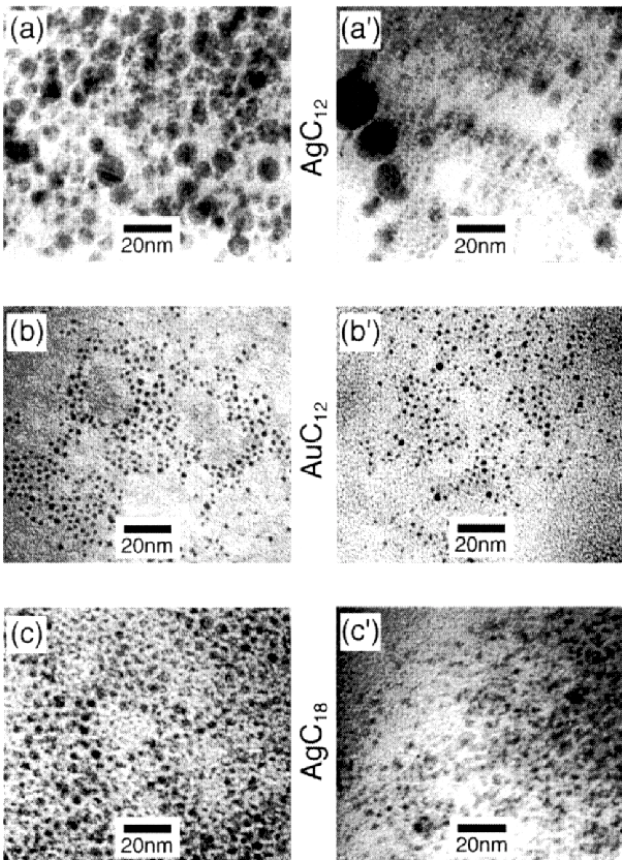

Fig. 3 TEM images of AgC_{12} (a), AuC_{12} (b), and AgC_{18} nanoparticles (c). The left and right ones of each sample were measured before and after, respectively, irradiation of 30-ps, 355-nm, 80-mW/cm^2 laser beam into each sample dispersed in cyclohexane. The irradiation times are 9 min for (a´) and 25 min for (b ´) and (c´).

transformation depends not only on the metal composition but also on the alkanethiol chain length. Irradiation induces AgC_{12} particles to decompose into fragments as small as 2 nm in diameter with much wider size distribution. Such fragmentation can be attributed to the absorption spectral change observed in Fig. 1. This can be understood by invoking the fact that the plasmon absorption should decrease and become broader as the size of nanoparticles decreases in the intrinsic size region [42,47]. The intrinsic size region of metal nanoparticles is the size smaller than about 10 nm in radius according to the Mie theory [47]. Figure 3a also shows that some particles become larger with irradiation than the initial ones. We suppose that the reduced solubility of the newly exposed alkanethiol-free side's enforces the fragments to combine to form enlarged particles. Later, they would aggregate further to turn into greater agglomerates. On this basis, the absorbance increase at an extremely long wavelength near 800 nm may be attributed to the longitudinal transition of the enlarged eccentric nanoparticles as well as to the broader scattering of the smaller fragments [36]. The spectra in Fig. 1a and the TEM images in Fig. 3a reveal that the particles after irradiation are very polydisperse with wide size and shape distributions. This suggests that shattering, rather than a successive transformation into smaller particles, takes place with irradiation for silver nanoparticles. However, Figs. 1c and 3b dictate that gold nanoparticles undergo shape transformation stepwise, presumably into energetically more stable shapes such as more spherical shape [46]. The initial increase of absorbance at the peak maximum wavelength for $AgAuC_{12}$ and AgC_{18} indicates that much the same type of phototransformation takes place in silver and bimetallic silver/gold nanoparticles as in gold nanoparticles. Nonetheless, it is evident that, as the molar fraction of gold atoms in bimetallic particles or the chain length of the alkanethiol increases, the irradiation time

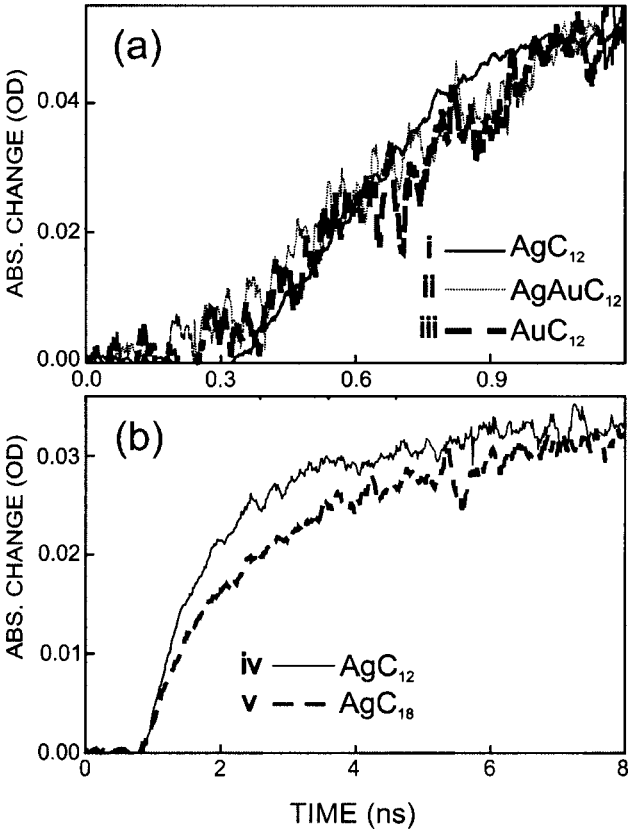

Fig. 4 Transient absorption formation kinetic profiles of noble metal nanoparticles dispersed in cyclohexane at two different time windows. Samples were excited with 0.8 mJ pulses of 355 nm and probed at 580 nm.

required to disintegrate particles to a same degree becomes longer. This implies that the fragmentation efficiency in a given irradiation time becomes concomitantly lower.

The transient absorption kinetic profiles are quite comparable to one another in a short time window. The rise time of 0.7 ns deconvoluted from the profiles of Fig. 4a is attributable to the conduction time of thermalized plasmon excitation energy to the passivant alkanethiol. The change in the dielectric constant of the surrounding medium caused by the conducted heat is supposed to modify the extinction coefficient of the nanoparticles to give rise to a transient absorption. In longer time windows, however, the kinetic profiles are subjected to a great change, depending on the metal composition as well as on the alkanethiol chain length. Besides the fast rise component of 0.7 ns the profiles **iv** and **v** of silver nanoparticles in Fig. 4b have slow rise components of 3.6 (13%) and 5.0 ns (48%), respectively. However, the profiles **i** and **iv** of bimetallic AgAu nanoparticles, as well as the profile **ii** of gold nanoparticles, in Fig. 5 show only the fast rise time of 0.7 ns with dual decay times. The profile **iii** of silver nanoparticles shows a slow single decay time with dual rise times. While the slow decay times are about 40 ns for all the profiles of Fig. 5, the fast decay times are 1.2 ns (88%) for **i**, 1.4 ns (97%) for **ii**, and 1.2 ns (88%) for **iv**. The fast decay times of gold and bimetallic nanoparticles are suggested to be the lifetimes of the refractive index transient artificially produced by the conducted heat with a further heat dissipation to the solvent molecules. On the other hand, the slow rise times for silver nanoparticles are attributed to the times that are needed for alkanethiol to dissipate the heat to reach the threshold thermal level, below which alkanethiol can not dissociate from the metal particle. Apparent transient absorption is seen to increase further because the excitation coefficient increases with dethiolation. As gold, as well as bimetallic, nanoparticles also show the slow decay component, both processes of dethiolation and

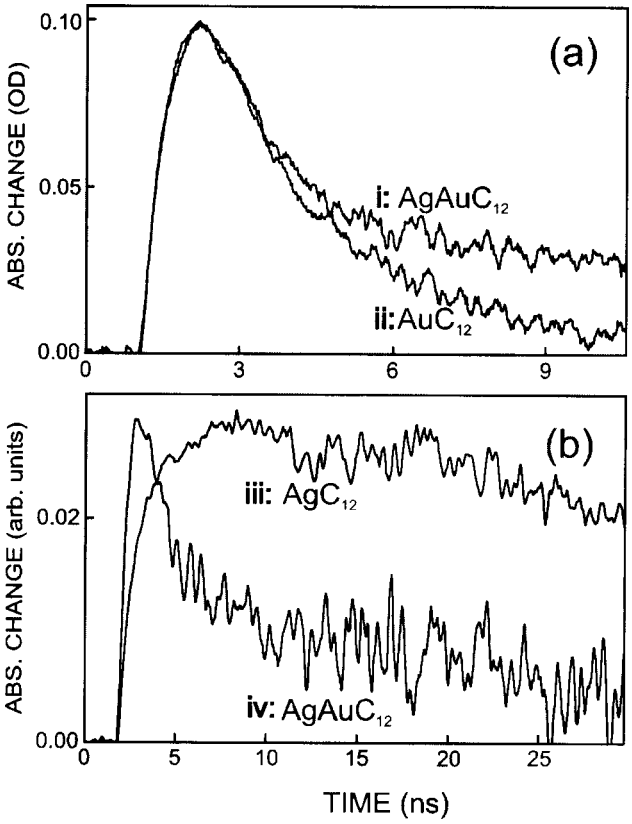

Fig. 5 Transient absorption decay kinetic profiles of noble metal nanoparticles in cyclohexane at two different time windows. Samples were excited with 0.8 mJ pulses of 355 nm and probed at 580 nm.

dielectric relaxation occur for all the noble metal nanoparticle systems we are reporting. The absorption increase induced by dethiolation is thus supposed to overwhelm the absorption decrease caused by dielectric relaxation for silver nanoparticles. The relative amplitudes of the two processes basically determine the overall transient absorption kinetic feature in the time range of several nanoseconds. It is our belief that the rise time of the dissociated transient is longer than the relaxation time of the artificial nonlinear refractive index transient, although both times are determined by the same heat dissipation rate. The drastic decrease of the relative amplitude of the slow decay component with the increase in the mole fraction of gold suggests that it is more difficult for alkanethiol to dissociate from gold than from silver. As seen in Figs. 1 and 2, some of the dethiolated particles are subject to disintegration before dissociated alkanethiols recombine to nanoparticles. The recombination takes place with the rate constant of $(40\ \text{ns})^{-1}$, which must be much larger than that of the fragmentation process, for the slow decay time is barely dependent on the kind of metal. The kinetic profile of AgC_{18} rises more slowly than the profile of AgC_{12} under the same experimental conditions. This can be understood by presuming that a longer alkyl chain retards the heat dissipation owing to a relatively slower motion. Although the observed heat dissipation time becomes longer, the smaller photolysis efficiency shown in Figs. 2 and 3 suggests that retardation with a longer stabilizer chain affects more significantly the dethiolation rate than the heat dissipation rate.

Figure 6 shows that the fragmentation efficiency of the silver particles depends strongly on solvent. The efficiency decreases with the increase in the dipole moment of the solvent molecules. Even after the thermalized photon energy has conducted to the immediately surrounding alkanethiol, it continuously dissipates to the solvent molecules. Dethiolation, which is a prerequisite to fragmentation,

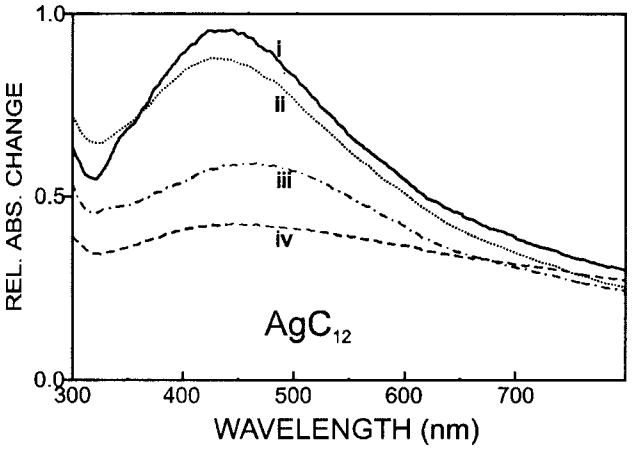

Fig. 6 Absorption spectra without and with irradiation of AgC_{12} in various solvents. The solvent for **i** and **iv** spectra is cyclohexane, that for **ii** is tetrahydrofuran, and that for **iii** is toluene. Whereas the spectrum of **i** was measured without irradiation, the spectra of **ii**, **iii**, and **iv** were measured after irradiation of 30-ps, 355-nm, 60-mW/cm^2 laser beam for 12 min.

should occur before the thermalized energy on alkanethiol dissipates to the solvent molecules. More polar solvent is supposed to expedite the thermal dissipation process, therefore the disintegration efficiency is lowered. The effect of the polar solvent is apparently the same as that of the alkyl chain length, although the latter effect is mainly to slow down the dethiolation rate.

Compared with silver nanoparticles, gold nanoparticles resist strongly against both dethiolation and subsequent fragmentation. We can describe several reasons for these differences. It is reported [3] that the accumulation of photoejected electrons at or near the surface leads to the disintegration of silver particles suspended in water. Considering this, we propose that the dissociation of alkanethiol occurs simultaneously with photoelectron ejection, giving positive charges to the particle, and that the charged particles subsequently experience disintegration prior to their recombination. Since the work function of gold (5.1 eV) is significantly higher than that of silver (4.3 eV) [21], it will be more difficult for a gold nanoparticle to eject a photoelectron. The lower oxidation potential of gold will also make the gold particle slowly undergo heterolytic dethiolation. In addition, the significantly larger molar enthalpy of atomization as well as the higher melting and boiling points of gold will reduce the occurrence of disintegration of dethiolated gold nanoparticles. Considered reported facts [21,46], polyhedral gold nanoparticles with thermalized excitation energy are supposed to melt to change into energetically more favorable shapes such as more spherical shape before the heat conducts to the surrounding medium. Admitting that the superficial shape of a sphere looks smaller than other shapes of the same mass, the size reduction and the aggregation observed with TEM images, together with the spectral changes, dictate that irradiation makes some atoms of gold nanoparticles vaporize and diffuse out. Diffused gold atoms aggregate later because of the low solubility of bare metals in cyclohexane [21,46]. If shape transformation via fusion and vaporization occurs in gold particles, it could also occur in silver particles as a result of the lower melting and boiling temperatures. Silver particles have larger heat capacities because of their larger sizes than gold particles, therefore the silver particles require more photon energy to melt and vaporize than the gold particles. It is not obvious from the TEM images whether much the same shape transformation prior to fragmentation occurs for silver particles like gold particles. However, the absorption increase and the spectral narrowing of the plasmon absorption with irradiation in the early time strongly suggest that the silver-contained nanoparticles also undergo reshaping via fusion and vaporization.

In summary, we have studied the kinetics and mechanism for the phototransformation phenomena of *n*-alkanethiol-derivatized nanoparticles by means of static and time-resolved absorption spectroscopy. The results are schematically presented in Fig. 7. Silver nanoparticles undergo fragmentation upon irradiation, while gold ones barely do. Silver/gold bimetallic composite nanoparticles follow the

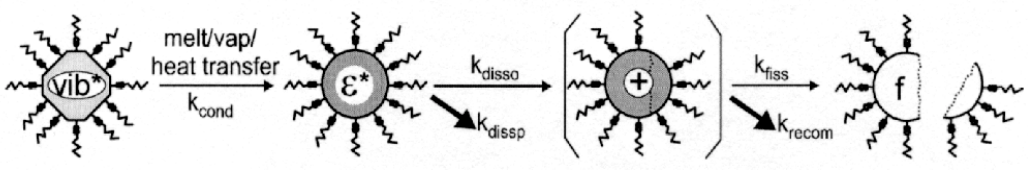

Fig. 7 Schematic diagram for the photon-initiated shape transformation of *n*-alkanethiol-derivatized noble metal nanoparticles dispersed in organic solvents. The degree of darkness symbolically represents the relative extent of absorption coefficient at each stage.

case of silver nanoparticles with a reduced efficiency. The fragmentation efficiency decreases as the chain length of derivatizing alkanethiol or the dipole moment of solvent molecule increases. Thermalized photon energy transfers to alkanethiol to change the dielectic constant of the surrounding medium. While artificial transient absorption arising from the refractive index change decays, a fraction of the excited nanoparticles experience a further absorption increase as hot alkanethiols dissociate. Dethiolation takes place until the transferred thermal energy of alkanethiol dissipates further in a time scale longer than the nonlinear dielectric relaxation time. Apparent transient absorption in a time scale of a few nanoseconds increases with time for silver nanoparticles while it decreases with time for gold and composite nanoparticles. These variations are due to the variations of the dethiolation efficiency. Some of the dethiolated particles are also subject to fragmentation until they recombine in a time scale of 40 ns. Shape transformation of gold nanoparticles is suggested to occur mainly via fusion and vaporization prior to the heat transfer of thermalized photon energy. The same type of transformation may also take place for silver nanoparticles but its effect is less apparent because of more significant fragmentation. The difference in the phototransformation of the two metals can be attributed to the differences in work function, oxidation potential, atomization enthalpy, and average particle size. In addition, smaller fragmentation efficiency with more polar solvent or longer alkanethiol chain can be associated with the relatively smaller dissociation rate compared with the competing dissipation rate.

ACKNOWLEDGMENT

This work was supported through the Research Institute of Molecular Science in Seoul National University and in part by the Brain Korea 21 program.

REFERENCES

1. M. M. Alvarez, J. T. Khoury, T. G. Schaaff, M. N. Shafigullin, I. Vezmar, R. L. Whetten. *J. Chem. Chem. B* **101**, 3706 (1997).
2. J. H. Hodak, I. Martini, G. V. Hartland. *J. Phys. Chem. B* **102**, 6958 (1998).
3. P. V. Kamat, M. Flumiani, G. V. Hartland. *J. Phys. Chem. B* **102**, 3123 (1998).
4. S. L. Logunov, T. S. Ahmadi, M. A. El-Sayed, J. T. Khoury, R. L. Whetten. *J. Phys. Chem. B* **101**, 3713 (1997).
5. (a) G. Schmid, H. West, H. Mehles, A. Lehnert. *Inorg. Chem.* **36**, 891 (1997). (b) M. S. Nashner, A. I. Frenkel, D. L. Adler, J. R. Shapley, R. G. Nuzzo. *J. Am. Chem. Soc.* **119**, 7760 (1997).
6. P. Mulvaney. In *Semiconductor Nanoclusters-Physical, Chemical and Catalytic Aspects*, P. V. Kamat, D. Meisel (eds.), p. 99, Elsevier Science, Amsterdam (1997).
7. J. Aizenberg, A. J. Black, G. M. Whitesides. *J. Am. Chem. Soc.* **121**, 4500 (1999).
8. T. Teranishi, M. Horsoe, T. Tanaka, M. Miyake. *J. Phys. Chem. B* **103**, 3818 (1999).

9. K. Torigoe and K. Esumi. *J. Phys. Chem. B* **103**, 2862 (1999).
10. M. B. Mohamed, K. Z. Ismail, S. Link, M. A. El-Sayed. *J. Phys. Chem. B* **102**, 9370 (1998).
11. J. M. Petroski, Z. L. Wang, T. C. Green, M. A. El-Sayed. *J. Phys. Chem. B* **102**, 3316 (1998).
12. Z. L. Wang, J. M. Petroski, T. C. Green, M. A. El-Sayed. *J. Phys. Chem. B* **102**, 6145 (1998).
13. S. Chen, T. Ida, K. Kimura. *J. Phys. Chem. B* **102**, 6169 (1998).
14. G. L. Hornyak, C. J. Patrissi, C. R. Martin. *J. Phys. Chem. B* **101**, 1548 (1997).
15. Y. -Y. Yu, S. -S Chang, C. -L. Lee, C. R. C.Wang. *J. Phys. Chem. B* **101**, 6661 (1997).
16. T. S. Ahmadi, Z. L. Wang, T. C. Green, A. Henglein M. A. El-Sayed. *Science* **272**, 1924 (1996).
17. K. V. Sarathy, G. Raina, R. T. Yadav, G. U. Kulkarni, N. R. Rao. *J. Phys. Chem. B* **101**, 9876 (1997).
18. M. T. Reetz and W. Helbig. *J. Am. Chem. Soc.* **116**, 7401 (1994).
19. C. A. Foss, Jr., G. L. Hornyak, J. A. Stockert, C. R. Martin. *J. Phys. Chem.* **98**, 2963 (1994).
20. H. Fujiwara, S. Yanagida, P. V. Kamat. *J. Phys. Chem. B* **103**, 2589 (1999).
21. A. Takami, H. Kurita, S. Koda. *J. Phys. Chem. B* **103**, 1226 (1999).
22. J. Hodak, I. Martini, G. V. Hartland. *Chem. Phys. Lett.* **284**, 135 (1998).
23. A. K. Boal and V. M. Rotello. *J. Am. Chem. Soc.* **121**, 4914 (1999).
24. R. M. Crooks and A. Ricco. *J. Acc. Chem. Res.* **31**, 219 (1998).
25. N. Toshima, T. Yonezawa, K. Kushihashi. *J. Chem. Soc. Faraday Trans.* **89**, 2537 (1993).
26. J. M. Thomas. *Pure Appl. Chem.* **60**, 1517 (1988).
27. S. Underwood and P. Mulvaney. *Langmuir* **10**, 3427 (1994).
28. M. J. Hostetler, C. -J. Zhong, B. K. H. Yen, J. Anderegg, S. M. Gross, N. D. Evans, M. Porter, R. W. Murray. *J. Am. Chem. Soc.* **120**, 9396 (1998).
29. S. Link and M. A. El-Sayed. *J. Phys. Chem. B* **103**, 4212 (1999).
30. S. Link, M. B. Mohamed, M. A. El-Sayed. *J. Phys. Chem. B* **103**, 3073 (1999).
31. S. Link, Z. L. Wang, M. A. El-Sayed. *J. Phys. Chem. B* **103**, 3529 (1999).
32. P. B. Johnson and R. W. Christy. *Phys. Rev. B* **6**, 4370 (1972).
33. B. Palpant, B. Prével, J. Lermé, E. Cottancin, M. Pellarin, M. Treilleux, A. Perez, J. L. Vialle, M. Broyer. *Phys. Rev. B* **57**, 1963 (1998).
34. S. W. Han, Y. Kim, K. Kim. *J. Colloid Interf. Sci.* **208**, 272 (1998).
35. B. M. I. van der Zande, M. R. Böhmer, L. G. J. Fokkink, C. Schönenberger. *J. Phys. Chem. B* **101**, 852 (1997).
36. P. Mulvaney. *Langmuir* **12**, 788 (1996).
37. M. T. Reetz, W. Heibig, S. A. Quaiser, U. Stimming, N. Breuer, R. Vogel. *Science* **267**, 367 (1995).
38. A. Henglein, B. G. Ershov, M. Malow. *J. Phys. Chem.* **99**, 14129 (1995).
39. A. Taleb, C. Petit, M. P. Pileni. *J. Phys. Chem. B* **102**, 2214 (1998).
40. T. Linnert, P. Mulvaney, A. Henglein. *J. Phys. Chem.* **97**, 679 (1993).
41. F. Strelow and A. Henglein. *J. Phys. Chem.* **99**, 11834 (1995).
42. S. Link and M. A. El-Sayed. *J. Phys. Chem. B* **103**, 8410 (1999).
43. A. Henglein and D. Meisel. *J. Phys. Chem. B* **102**, 8364 (1998).
44. S. Y. Kang and K. Kim. *Langmuir* **14**, 226 (1998).
45. D. -J. Jang and D. F. Kelley. *Rev. Sci. Instrum.* **56**, 2205 (1985).
46. S. Link, C. Burda, M. B. Mohamed, B. Nikoobakht, M. A. El-Sayed. *J. Phys. Chem. B* **103**, 1165 (1999).
47. U. Kreibig and M. Vollmer. *Optical Properties of Metal Clusters*, Chapter 2, Springer, Berlin (1995).